molecules

MDPI

Article

# Elucidating Direct Photolysis Mechanisms of Different Dissociation Species of Norfloxacin in Water and $Mg^{2+}$ Effects by Quantum Chemical Calculations

**Se Wang * and Zhuang Wang ***

Collaborative Innovation Center of Atmospheric Environment and Equipment Technology, Jiangsu Key Laboratory of Atmospheric Environment Monitoring and Pollution Control, School of Environmental Science and Engineering, Nanjing University of Information Science and Technology, Nanjing 210044, China
* Correspondence: wangse@nuist.edu.cn (S.W.); zhuang.wang@nuist.edu.cn (Z.W.)

Received: 1 November 2017; Accepted: 8 November 2017; Published: 11 November 2017

**Abstract:** The study of pollution due to combined antibiotics and metals is urgently needed. Photochemical processes are an important transformation pathway for antibiotics in the environment. The mechanisms underlying the effects of metal-ion complexation on the aquatic photochemical transformation of antibiotics in different dissociation forms are crucial problems in science, and beg solutions. Herein, we investigated the mechanisms of direct photolysis of norfloxacin (NOR) in different dissociation forms in water and metal ion $Mg^{2+}$ effects using quantum chemical calculations. Results show that different dissociation forms of NOR had different maximum electronic absorbance wavelengths ($NOR^{2+}$ < $NOR^{0}$ < $NOR^{+}$) and showed different photolysis reactivity. Analysis of transition states (TS) and reaction activation energies ($E_a$) indicated $NOR^{+}$ generally underwent loss of the piperazine ring (C10–N13 bond cleavage) and damage to piperazine ring (N13–C14 bond cleavage). For $NOR^{2+}$, the main direct photolysis pathways were de-ethylation (N7–C8 bond cleavage) and decarboxylation (C2–C5 bond cleavage). Furthermore, the presence of $Mg^{2+}$ changed the order of the wavelength at maximum electronic absorbance ($NOR^{+}$-$Mg^{2+}$ < $NOR^{0}$-$Mg^{2+}$ < $NOR^{2+}$-$Mg^{2+}$) and increased the intensities of absorbance peaks of all three dissociation species of NOR, implying that $Mg^{2+}$ played an important role in the direct photolysis of $NOR^{0}$, $NOR^{+}$, and $NOR^{2+}$. The calculated TS results indicated that the presence of $Mg^{2+}$ increased $E_a$ for most direct photolysis pathways of NOR, while it decreased $E_a$ for some direct photolysis pathways such as the loss of the piperazine ring and the damage of the piperazine ring of $NOR^{0}$ and the defluorination of $NOR^{+}$.

**Keywords:** norfloxacin; direct photolysis pathways; DFT; ionic forms; $Mg^{2+}$

## 1. Introduction

Antibiotics are widely used in aquaculture, animal husbandry, and medical treatment, due to the fact that they can either kill or inhibit the growth of bacteria [1,2]. Antibiotics are frequently released into the environment due to negligence, and they are frequently detected in the aquatic environment [1,3]. Norfloxacin (NOR) was the first fluoroquinolone antibiotic to be used clinically [4], and has been found to be one of the most frequently detected fluoroquinolone antibiotics in surface waters [5–8] and municipal wastewater [9]. Recently, a lot of attention has also been devoted to studies on the behavior, fate, and degradation methods of NOR in the aquatic environment [10–12].

Photolysis is expected to play an important role in determining the fate and behavior of fluoroquinolone antibiotics including NOR in some sunlit surface waters [13–18]. Photolysis includes direct and indirect photolysis. For the direct photolysis of organic pollutants, a molecule itself absorbs photons and is degraded [19]. Indirect photolysis may include reaction with transient excited species such as singlet oxygen, hydroxyl radical, triplet excited state dissolved organic matter, or other reactive

species [20]. The UV-Vis absorption spectrum of NOR consists of one major peak at 276 nm and a broad band at approximately 300 to 350 nm [21], which indicates that NOR can undergo direct photolysis in the aquatic environment. The molecular structure of NOR contains ionizable groups (–COOH, $–NH_n$), resulting in the aqueous presence of NOR in various dissociation states. Previous studies have indicated that the photolysis rate of NOR is greatly influenced by the pH of the solution [10,11]. However, the mechanisms underlying the direct photolysis of NOR in different dissociation forms have not yet been fully understood.

Recently, issues related to the study of pollution resulting from the combination of antibiotics and metals have been drawing a lot of attention [20,22,23]. Previous studies have suggested that metal ions such as $Mg^{2+}$ can have an effect on the photochemical behavior of organic pollutants [20,24]. For example, Werner et al. [22] found that the direct photolysis rate constant of tetracycline was greatly influenced by the presence of $Ca^{2+}$ or $Mg^{2+}$. Martínez et al. [23] found that metal cations may affect the photochemical properties of NOR. Metal ion $Mg^{2+}$ occurs at a high concentration in natural water environment [25]. Following the environmental release of NOR, there may be interactions between NOR and $Mg^{2+}$. Thus, the mechanisms of $Mg^{2+}$'s effect on the photolysis of different dissociation species of NOR urgently need to be investigated.

Obtaining experimental data can be laborious, costly, and time-consuming. Quantum chemistry calculations have been found to be efficient alternatives for predicting the environmental behavior and fate of organic pollutants, and for providing an important information on reaction intermediates or reactive species involved in chemical reactions that are difficult to be detected experimentally [26–31]. It was the purpose of this study to investigate the direct photolysis mechanisms of different dissociation species of NOR in water and $Mg^{2+}$ effects based on density functional theory (DFT).

## 2. Computational Methods

NOR was selected as a model compound (Figure 1). The geometry optimization of all structures in solvent water was carried out using DFT [32] and Becke's three-parameter hybrid exchange function with Lee-Yang-Parr gradient-corrected correlation functional (B3LYP) [33] with 6-311+G (d,p) basis set. The integral equation formalism of polarized continuum model (IEFPCM) was employed to consider the solvent effects in water [34]. The UV absorbance spectra of different ionic forms of NOR and complexes with $Mg^{2+}$ in water were calculated using time-dependent density functional theory (TDDFT) at B3LYP/6-311++G (d,p) level [35–37].

The possible direct photolysis reaction pathways were calculated at the lowest excited triplet states, as the lowest excited triplet states have been found to be long-lived photochemical reaction precursors for many compounds [38]. The direct photolysis reaction pathways of different ionic forms of NOR and complexes with $Mg^{2+}$ in solvent water were calculated employing the DFT method at the B3LYP/6-311+G (d,p) level of theory. The geometries at the lowest triplet states were calculated with a spin multiplicity of 3. Frequency calculations were performed at the same level to confirm all the stationary points. Transition states (TS) were characterized with one imaginary vibrational frequency. Intrinsic reaction coordinate (IRC) calculations were performed to confirm that TS do connect with the corresponding reactants and products [39]. Zero-point energy correction was considered for the estimated reaction activation energy. All calculations were carried out using the Gaussian 09 software package (Rev. B. 01; Gaussian Inc.: Wallingford, CT, USA) [40].

## 3. Results and Discussion

### *3.1. Geometries of Three Dissociation Species (*$NOR^0$, $NOR^+$, *and* $NOR^{2+}$*) in Water*

NOR may exhibit five dissociation species with $pK_{a,1}$ (3.11 ± 0.30), $pK_{a,2}$ (6.10 ± 0.19), $pK_{a,3}$ (8.60 ± 0.10), and $pK_{a,4}$ (10.56 ± 0.30) in water [41], of which three dissociation species $NOR^0$, $NOR^+$, $NOR^{2+}$ are dominant in natural water environments, and were thus investigated in the present study (Figure 1). The optimized geometries of the three environmentally relevant dissociation species

$NOR^0$, $NOR^+$, and $NOR^{2+}$ are presented in Figure 2. There are differences among the geometries of the three dissociation species, to some extent. For instance, the bond length of N7–C8 of $NOR^{2+}$ (1.565 Å) is longer than that of $NOR^0$ (1.486 Å)/$NOR^+$ (1.489 Å). The bond length of C10–N13 of $NOR^+$ (1.481 Å)/$NOR^{2+}$ (1.478 Å) is longer than that of $NOR^0$ (1.407 Å). The bond length of N13–C14 of $NOR^+$ (1.523 Å)/$NOR^{2+}$ (1.529 Å) is longer than that of $NOR^0$ (1.471 Å). The dihedral angle O3–C2–C5–C6 of $NOR^+$ (47.0°) is similar to that of $NOR^0$ (52.8°). However, the dihedral angle O3–C2–C5–C6 of $NOR^{2+}$ is 89.4°, indicating that the plane of O3–C2 bond is nearly orthogonal to the plane of C5–C6 bond. Additionally, the computed electronic absorption spectra of the three dissociation forms of NOR in water are shown in Figure 3a. The order of the computed wavelength at maximum electronic absorbance of the three dissociation species in water is $NOR^{2+}$ (280 nm) < $NOR^0$ (282 nm) < $NOR^+$ (308 nm) at TDDFT/B3LYP/6-311++G (d,p) level. The corresponding experimental data is around 275 nm in water (pH = 7.0) [21] and 274 nm in water (pH = 7.4) [23].

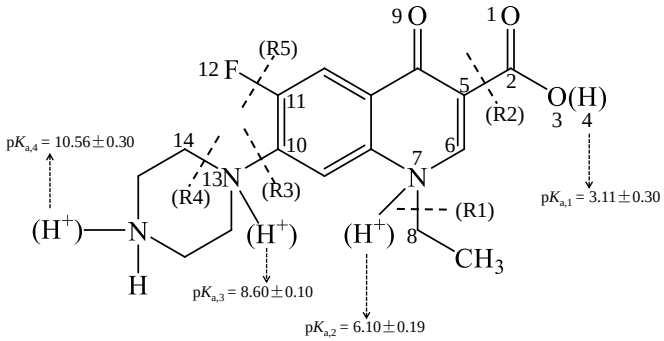


**Figure 1.** Structural formulae of norfloxacin (NOR) and numbering scheme for atomic positions. The p$K_a$ values are taken from ref. [41].

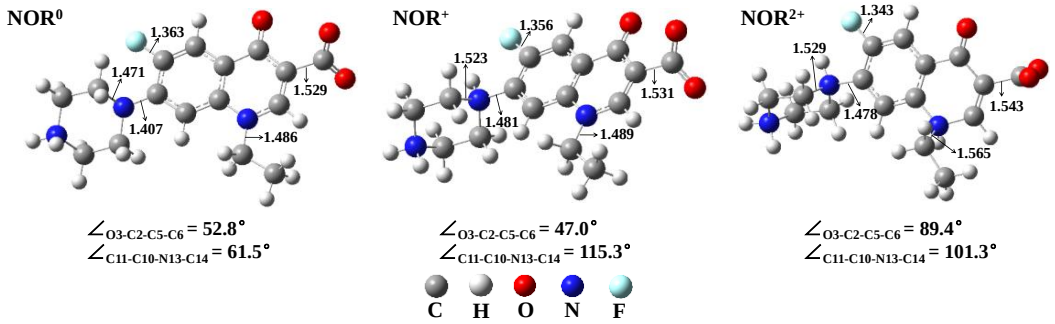


**Figure 2.** Optimized geometries of three dissociation species of NOR, along with selected bond lengths (Å) and dihedral angles (°).

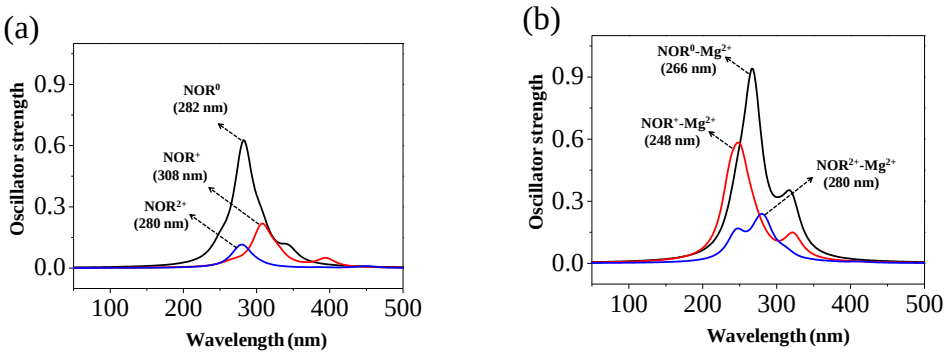


**Figure 3.** Calculated electronic absorption spectra of (**a**) NOR and (**b**) complexes NOR-$Mg^{2+}$.

### 3.2. Direct Photolysis Pathways of Three Dissociation Species ($NOR^0$, $NOR^+$, and $NOR^{2+}$) in Water

As depicted in Figure 1, five possible reaction pathways were considered in the calculation of direct photolysis of NOR at the excited triplet states, including de-ethylation (N7–C8 bond cleavage/R1), decarboxylation (C2–C5 bond cleavage/R2), loss of piperazine ring (C10–N13 bond cleavage/R3), damage of piperazine ring (N13–C14 bond cleavage/R4), and defluorination (C11–F12 bond cleavage/R5). The computed reaction activation energies ($E_a$, kcal·mol$^{-1}$) for the five photolysis reaction pathways in different dissociation forms are listed in Table 1. The optimized geometries of reaction TS are shown in Figures 4, S1 and S2.

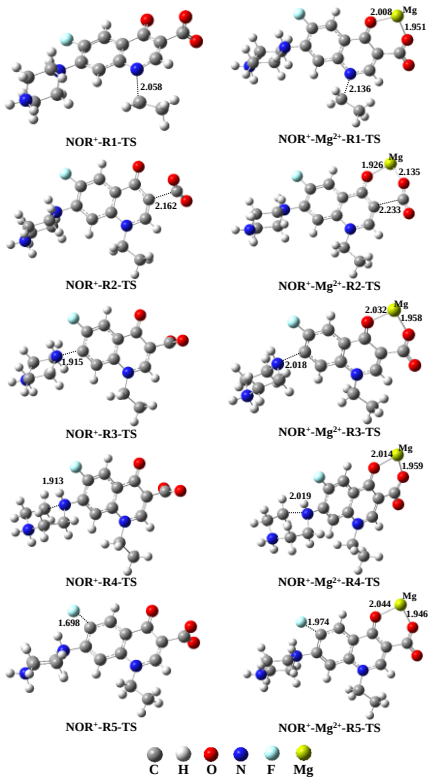


**Figure 4.** The transition state geometries of direct photolysis pathways R1, R2, R3, R4, and R5 of $NOR^+$ and $NOR^+$-$Mg^{2+}$.

**Table 1.** Computed activation energies ($E_a$, kcal·mol$^{-1}$) for the five photolysis reaction pathways (R1, R2, R3, R4, and R5) of three dissociation forms of NOR and complexes with $Mg^{2+}$.

| | R1 (Cleavage of N7–C8 Bond) | R2 (Cleavage of C2–C5 Bond) | R3 (Cleavage of C10–N13 Bond) | R4 (Cleavage of N13–C14 Bond) | R5 (Cleavage of C11–F12 Bond) |
|---|---|---|---|---|---|
| $NOR^0$ | 21.0 | 27.6 | 31.2 | 26.3 | - |
| $NOR^0$-$Mg^{2+}$ | 23.0 | 36.5 | 26.3 | 18.6 | - |
| $NOR^+$ | 25.4 | 23.0 | 9.5 | 7.7 | 18.7 |
| $NOR^+$-$Mg^{2+}$ | 27.9 | 31.2 | 17.1 | 12.7 | 11.4 |
| $NOR^{2+}$ | 5.4 | 8.9 | 30.0 | 20.5 | 42.5 |
| $NOR^{2+}$-$Mg^{2+}$ | 5.2 | 12.5 | 35.3 | 27.3 | 55.4 |

"-" represents transition state and corresponding reaction activation energy were not available.

As can be seen from Table 1, the $E_a$ values of pathway R3 (9.5 kcal·mol$^{-1}$) and R4 (7.7 kcal·mol$^{-1}$) for $NOR^+$ are obviously lower than those of other pathways. Thus, pathways R3 and R4 are easier to carry out than other pathways, and are the main pathways for the direct photolysis of $NOR^+$. Additionally, the $E_a$ value of pathway R1 (25.4 kcal·mol$^{-1}$) for $NOR^+$ is the highest of all the five

photolysis pathways, indicating that the cleavage of the N7–C8 bond (de-ethylation) is the hardest to overcome among the five pathways.

For dissociation form $NOR^{2+}$, the $E_a$ values of pathway R1 (5.4 kcal·mol$^{-1}$) and R2 (8.9 kcal·mol$^{-1}$) are remarkably lower than those of other pathways (Table 1), revealing that de-ethylation and decarboxylation are the main pathways for the direct photolysis of $NOR^{2+}$. In addition, the $E_a$ value of pathway R5 is too high (42.5 kcal·mol$^{-1}$) (Table 1), indicating that $NOR^{2+}$ is difficult to defluorinate via the cleavage of the C11–F12 bond. For neutral dissociation form $NOR^0$, the $E_a$ value of pathway R1 (21.0 kcal·mol$^{-1}$) is the lowest, while the $E_a$ value of pathway R3 (31.2 kcal·mol$^{-1}$) is the highest among all the pathways. Thus, $NOR^0$ is difficult to take off the piperazine ring via cleavage of C10–N13 bond. Taken together, $NOR^{2+}$ is the easiest to de-ethylate via the cleavage of the N7–C8 bond among the three dissociation species, and are easier to undergo the cleavage of the C2–C5 bond (decarboxylation) than the other two dissociation species. In addition, $NOR^+$ is the easiest with which to carry out the cleavage of the C10–N13/N13–C14 bond among the three dissociation species. Thus, the photochemical reactivities of the different dissociation species of NOR are quite different from each other.

### *3.3. Complex Geometries of Three Dissociation Species ($NOR^0$, $NOR^+$, and $NOR^{2+}$) with Metal Ion $Mg^{2+}$ in Water*

Optimized geometries of the complex NOR-$Mg^{2+}$ are shown in Figure 5 and Figures S3 and S4. Computed results indicate that complex $NOR^+$-$Mg^{2+}$ has four possible geometries. $NOR^+$-$Mg^{2+}$ (1) is the most stable geometry with the lowest single point energy among the four geometries, and is the main geometry discussed in this research (Figure 5). The results also indicate that $NOR^0$-$Mg^{2+}$ (1) and $NOR^{2+}$-$Mg^{2+}$ (1) are the most stable geometries (Figures S3 and S4). All the following calculations are based on the structure $NOR^0$-$Mg^{2+}$ (1), $NOR^+$-$Mg^{2+}$ (1), and $NOR^{2+}$-$Mg^{2+}$ (1).

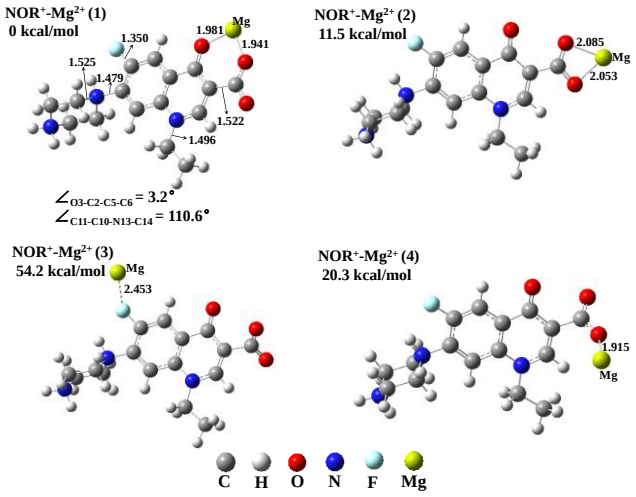


**Figure 5. Four** optimized geometries (1), (2), (3), (4) of complex $NOR^+$-$Mg^{2+}$ along with selected bond lengths (Å) and dihedral angles (°). The energies of geometries are relative to that of the most stable geometry $NOR^+$-$Mg^{2+}$ (1).

The dihedral angle O3–C2–C5–C6 of the monomer $NOR^+$ and $NOR^0$ is 47.0° and 52.8° (Figure 2), while for complexes with $Mg^{2+}$ the dihedral angle O3–C2–C5–C6 is obviously reduced to 3.2° and 0.0° due to the formation of O1–Mg bond and O9–Mg bond (Figures 5 and S3). In complexes $NOR^+$-$Mg^{2+}$ and $NOR^0$-$Mg^{2+}$ the O3–C2 bond and C5–C6 bond is almost in a plane. In addition, with the formation of O1–Mg bond and O9–Mg bond in complex $NOR^{2+}$-$Mg^{2+}$, the dihedral angle O3–C2–C5–C6 is also dramatically reduced to 11.9° from 89.4° in monomer (Figures 2 and S4). The plane of the O3–C2 bond is nearly orthogonal to the plane of the C5–C6 bond in monomer $NOR^{2+}$, while the plane of the O3–C2

bond tends to be parallel to the plane of the C5–C6 bond in complex $NOR^{2+}$-$Mg^{2+}$. Additionally, the bond lengths of complexes are also different from those of monomers. For instance, the bond length of N13–C14/N7–C8 in complex $NOR^{+}$-$Mg^{2+}$ is longer than that in monomer $NOR^{+}$, while the bond length of C11–F12/C10–N13/C2–C5 in complex $NOR^{+}$-$Mg^{2+}$ is shorter than that in monomer $NOR^{+}$ (Figures 2 and 5).

The UV absorbance spectra of complexes with $Mg^{2+}$ in water were calculated using TDDFT at B3LYP/6-311++G (d,p) level (Figure 3b). The calculation results show that a blue shift occurs at the maximum electronic absorbance peaks of $NOR^{0}$-$Mg^{2+}$ and $NOR^{+}$-$Mg^{2+}$, compared with that of corresponding monomer. Additionally, $Mg^{2+}$ changes the order of maximum electronic absorbance wavelength of the three dissociation species. The order of maximum electronic absorbance wavelengths of complexes is: $NOR^{+}$-$Mg^{2+}$ (248 nm) < $NOR^{0}$-$Mg^{2+}$ (266 nm) < $NOR^{2+}$-$Mg^{2+}$ (280 nm). Additionally, with the presence of $Mg^{2+}$, there is an increase of 49.9%, 167.3%, and 108.0% in the intensities of absorption peaks for the three dissociation species $NOR^{0}$, $NOR^{+}$, and $NOR^{2+}$, respectively. The experimental results of Martínez et al. [23] also showed that the intensity of maximum absorption peak (274 nm) of NOR at pH = 7.4 is increased by around 42.6% when $Mg^{2+}$ is present. Thus, the metal ion $Mg^{2+}$ has an impact on both the structures and UV absorbance spectra of different dissociation species of NOR, which may also have an impact on direct photolysis of different dissociation species of NOR.

### *3.4. Effects of* $Mg^{2+}$ *on Direct Photolysis of Three Dissociation Species (*$NOR^{0}$, $NOR^{+}$, *and* $NOR^{2+}$*) in Water*

Five possible reaction pathways were considered in the calculation of direct photolysis of complexes NOR-$Mg^{2+}$ at the excited triplet states, including de-ethylation (N7–C8 bond cleavage/R1), decarboxylation (C2–C5 bond cleavage/R2), loss of piperazine ring (C10–N13 bond cleavage/R3), damage of piperazine ring (N13–C14 bond cleavage/R4), and defluorination (C11–F12 bond cleavage/R5). The computed activation energies ($E_a$, kcal·mol$^{-1}$) for the five photolysis reaction pathways in different dissociation forms are listed in Table 1. The optimized geometries of reaction TS are shown in Figures 4, S1 and S2.

For the complex $NOR^{+}$-$Mg^{2+}$, the computed $E_a$ values of four pathways (R1, R2, R3, and R4) are all higher than those of monomer $NOR^{+}$, indicating that $Mg^{2+}$ hinders the cleavage of the N7–C8 bond, C2–C5 bond, C10–N13 bond, and N13–C14 bond (Table 1). However, $Mg^{2+}$ promotes defluorination via the cleavage of the C11–F12 bond due to the lower $E_a$ value of reaction R5 compared with that of the monomer. Additionally, $Mg^{2+}$ also changes the main photolysis pathway of $NOR^{+}$. For monomer $NOR^{+}$, the damage of piperazine ring via the cleavage of N13–C14 bond is the easiest to occur due to the lowest $E_a$ value among all the five pathways. However, for complex $NOR^{+}$-$Mg^{2+}$, the $E_a$ value of R5 (defluorination) is the lowest among all the five pathways.

For the complex $NOR^{2+}$-$Mg^{2+}$, $Mg^{2+}$ has little impact on the $E_a$ value of pathway R1, while $Mg^{2+}$ significantly increases the $E_a$ value of pathways R2, R3, R4, and R5 (Table 1). Furthermore, the calculation results indicate that the main direct photolysis pathways are not changed by adding $Mg^{2+}$, implying that, for both monomer and complex, pathway R1 (cleavage of N7–C8 bond) is the most easily occurring among the five direct photolysis pathways for $NOR^{2+}$.

For the complex $NOR^{0}$-$Mg^{2+}$, the $E_a$ values of pathways R1and R2 are higher than those for the monomer $NOR^{0}$, while the $E_a$ values of pathways R3 and R4 are obviously lower than those for monomer $NOR^{0}$. $Mg^{2+}$ inhibits the cleavage of the N7–C8 bond and C2–C5 bond, but promotes the cleavage of the C10–N13 bond and N13–C14 bond. Furthermore, for the monomer $NOR^{0}$, the cleavage of the N7–C8 bond (pathway R1) is the most easily occurring among the four photolysis pathways, but for the complex $NOR^{0}$-$Mg^{2+}$, the cleavage of the N13–C14 bond (pathway R4) is the most easily occurring.

With the increase of pH, the dominant dissociation species is, in turn, $NOR^{0}$, $NOR^{+}$, and $NOR^{2+}$. As can be seen from Table 1, for de-ethylation (N7–C8 bond cleavage/R1), the order of $E_a$ is $NOR^{2+}$ < $NOR^{0}$ < $NOR^{+}$, which is not changed by the presence of $Mg^{2+}$. For decarboxylation (C2–C5 bond

cleavage/R2), the order of $E_a$ is $NOR^{2+}$ < $NOR^{+}$ < $NOR^{0}$, which is not changed by the presence of $Mg^{2+}$. For both the loss of the piperazine ring (C10–N13 bond cleavage/R3) and the damage of the piperazine ring (N13–C14 bond cleavage/R4), the order of $E_a$ is $NOR^{+}$ < $NOR^{2+}$ < $NOR^{0}$, which is changed by the presence of $Mg^{2+}$ ($NOR^{+}$-$Mg^{2+}$ < $NOR^{0}$-$Mg^{2+}$ < $NOR^{2+}$-$Mg^{2+}$). For defluorination (C11–F12 bond cleavage/R5), the order of $E_a$ is $NOR^{+}$ < $NOR^{2+}$, which is not changed by the presence of $Mg^{2+}$.

## 4. Conclusions

In summary, the computed TS and $E_a$ indicated that $NOR^{0}$, $NOR^{+}$, and $NOR^{2+}$ showed disparate photochemical reactivity in water. The main photolysis pathways for $NOR^{+}$ were the loss of the piperazine ring via the cleavage of the C10–N13 bond and the damage of the piperazine ring via the cleavage of the N13–C14 bond. The main pathways for $NOR^{2+}$ were de-ethylation via the cleavage of the N7–C8 bond and decarboxylation via the cleavage of the C2–C5 bond. In addition, the presence of $Mg^{2+}$ altered the electronic absorption spectra of NOR and increased the intensities of absorbance peaks of NOR. The TS results demonstrated that $Mg^{2+}$ had dual effects, as it can inhibit or promote the direct photolysis reactions of NOR. Quantum mechanics and density functional theory are potential tools for elucidating the mechanism of photochemical transformation of antibiotics in the water environment.

**Supplementary Materials:** Supplementary data associated with this article can be found, in the online version.

**Acknowledgments:** This research was supported by the National Natural Science Foundation of China (41601519 and 21407080), the Natural Science Foundation of Jiangsu Province (BK20150891 and BK20140987), and the Startup Foundation for Introducing Talent of Nanjing University of Information Science and Technology (2015r011). We thank the reviewers for their valuable comments on the manuscript.

**Author Contributions:** Se Wang planned the research, performed the theoretical computation, and co-wrote the paper; Zhuang Wang supervised the research and co-wrote the paper.

**Conflicts of Interest:** The authors declare no conflict of interest.

## References

1. Kümmerer, K. Antibiotics in the aquatic environment—A review—Part I. *Chemosphere* **2009**, *75*, 417–434. [CrossRef] [PubMed]
2. Pan, M.; Chu, L.M. Fate of antibiotics in soil and their uptake by edible crops. *Sci. Total Environ.* **2017**, *599*, 500–512. [CrossRef] [PubMed]
3. Zuccato, E.; Castiglioni, S.; Bagnati, R.; Melis, M.; Fanelli, R. Source, occurrence and fate of antibiotics in the Italian aquatic environment. *J. Hazard. Mater.* **2010**, *179*, 1042–1048. [CrossRef] [PubMed]
4. Moellering, R.C. Norfloxacin: A fluoroquinolone carboxylic acid antimicrobial agent. *Am. J. Med.* **1987**, *82*, 1–92. [CrossRef]
5. Watkinson, A.J.; Murby, E.J.; Kolpin, D.W.; Costanzo, S.D. The occurrence of antibiotics in an urban watershed: From wastewater to drinking water. *Sci. Total Environ.* **2009**, *407*, 2711–2723. [CrossRef] [PubMed]
6. Xu, W.; Zhang, G.; Zou, S.; Ling, Z.; Wang, G.; Yan, W. A preliminary investigation on the occurrence and distribution of antibiotics in the Yellow River and its tributaries, China. *Water Environ. Res.* **2009**, *81*, 248–254. [CrossRef] [PubMed]
7. Yao, L.; Wang, Y.; Tong, L.; Li, Y.; Deng, Y.; Guo, W.; Gan, Y. Seasonal variation of antibiotics concentration in the aquatic environment: A case study at Jianghan Plain, central China. *Sci. Total Environ.* **2015**, *527–528*, 56–64. [CrossRef] [PubMed]
8. Wang, W.; Wang, H.; Zhang, W.; Liang, H.; Gao, D. Occurrence, distribution, and risk assessment of antibiotics in the Songhua River in China. *Environ. Sci. Pollut. Res.* **2017**, *24*, 19282–19292. [CrossRef] [PubMed]
9. Zhang, X.; Zhao, H.; Du, J.; Qu, Y.; Shen, C.; Tan, F.; Chen, J.; Quan, X. Occurrence, removal, and risk assessment of antibiotics in 12 wastewater treatment plants from Dalian, China. *Environ. Sci. Pollut. Res.* **2017**, *24*, 16478–16487. [CrossRef] [PubMed]
10. Zhang, J.; Fu, D.; Wu, J. Photodegradation of Norfloxacin in aqueous solution containing algae. *J. Environ. Sci.* **2012**, *24*, 743–749. [CrossRef]

11. Ahmad, I.; Bano, R.; Musharraf, S.G.; Sheraz, M.A.; Ahmed, S.; Tahir, H.; ulArfeen, Q.; Bhatti, M.S.; Shad, Z.; Hussain, S.F. Photodegradation of norfloxacin in aqueous and organic solvents: A kinetic study. *J. Photoch. Photobiol. A* **2015**, *302*, 1–10. [CrossRef]
12. Santos, L.V.d.S.; Meireles, A.M.; Lange, L.C. Degradation of antibiotics norfloxacin by Fenton, UV and UV/$H_2O_2$. *J. Environ. Manag.* **2015**, *154*, 8–12. [CrossRef] [PubMed]
13. Ge, L.; Chen, J.; Wei, X.; Zhang, S.; Qiao, X.; Cai, X.; Xie, Q. Aquatic photochemistry of fluoroquinolone antibiotics: Kinetics, pathways, and multivariate effects of main water constituents. *Environ. Sci. Technol.* **2010**, *44*, 2400–2405. [CrossRef] [PubMed]
14. Li, Y.; Niu, J.; Wang, W. Photolysis of enrofloxacin in aqueous systems under simulated sunlight irradiation: Kinetics, mechanism and toxicity of photolysis products. *Chemosphere* **2011**, *85*, 892–897. [CrossRef] [PubMed]
15. Babić, S.; Periša, M.; Škorić, I. Photolytic degradation of norfloxacin, enrofloxacin and ciprofloxacin in various aqueous media. *Chemosphere* **2013**, *91*, 1635–1642. [CrossRef] [PubMed]
16. Wammer, K.H.; Korte, A.R.; Lundeen, R.A.; Sundberg, J.E.; McNeill, K.; Arnold, W.A. Direct photochemistry of three fluoroquinoloneantibacterials: Norfloxacin, ofloxacin, and enrofloxacin. *Water Res.* **2013**, *47*, 439–448. [CrossRef] [PubMed]
17. Wei, X.; Chen, J.; Xie, Q.; Zhang, S.; Ge, L.; Qiao, X. Distinct photolytic mechanisms and products for different dissociation species of ciprofloxacin. *Environ. Sci. Technol.* **2013**, *47*, 4284–4290. [CrossRef] [PubMed]
18. Liang, C.; Zhao, H.; Deng, M.; Quan, X.; Chen, S.; Wang, H. Impact of dissolved organic matter on the photolysis of the ionizable antibiotic norfloxacin. *J. Environ. Sci.* **2015**, *27*, 115–123. [CrossRef] [PubMed]
19. Zepp, R.G.; Cline, D.M. Rates of direct photolysis in aquatic environment. *Environ. Sci. Technol.* **1977**, *11*, 359–366. [CrossRef]
20. Wang, S.; Song, X.; Hao, C.; Gao, Z.; Chen, J.; Qiu, J. Elucidating triplet-sensitized photolysis mechanisms of sulfadiazine and metal ions effects by quantum chemical calculations. *Chemosphere* **2015**, *122*, 62–69. [CrossRef] [PubMed]
21. Zhang, P.; Li, H.; Yao, S.; Wang, W. Effects of pH and polarity on the excited states of norfloxacin and its 4′-*N*-acetyl derivative: A steady-state and time-resolved study. *Sci. China Chem.* **2014**, *57*, 409–416. [CrossRef]
22. Werner, J.J.; Arnold, W.A.; Mcneill, K. Water hardness as a photochemical parameter: Tetracycline photolysis as a function of calcium concentration, magnesium concentration, and pH. *Environ. Sci. Technol.* **2006**, *40*, 7236–7241. [CrossRef] [PubMed]
23. Martínez, L.; Bilski, P.; Chignell, C.F. Effect of magnesium and calcium complexation on the photochemical properties of norfloxacin. *Photochem. Photobiol.* **1996**, *64*, 911–917. [CrossRef]
24. Wang, S.; Song, X.; Hao, C.; Gao, Z.; Chen, J.; Qiu, J. Elucidating photodehalogenation mechanisms of polychlorinated and polybrominated dibenzo-*p*-dioxins and dibenzofurans and $Mg^{2+}$ effects by quantum chemical calculations. *Comput. Theor. Chem.* **2014**, *1042*, 49–56. [CrossRef]
25. Hafuka, A.; Yoshikawa, H.; Yamada, K.; Kato, T.; Takahashi, M.; Okabe, S.; Satoh, H. Application of fluorescence spectroscopy using a novel fluoroionophore for quantification of zinc in urban runoff. *Water Res.* **2014**, *54*, 12–20. [CrossRef] [PubMed]
26. Sabljic, A. QSAR models for estimating properties of persistent organic pollutants required in evaluation of their environmental fate and risk. *Chemosphere* **2001**, *43*, 363–375. [CrossRef]
27. Wang, S.; Hao, C.; Gao, Z.; Chen, J.; Qiu, J. Effects of excited-state structures and properties on photochemical degradation of polybrominated diphenyl ethers: A TDDFT study. *Chemosphere* **2012**, *88*, 33–38. [CrossRef] [PubMed]
28. Wang, S.; Hao, C.; Gao, Z.; Chen, J.; Qiu, J. Theoretical investigation on photodechlorination mechanism of polychlorinated biphenyls. *Chemosphere* **2014**, *95*, 200–205. [CrossRef] [PubMed]
29. Wang, S.; Hao, C.; Gao, Z.; Chen, J.; Qiu, J. Theoretical investigations on direct photolysis mechanisms of polychlorinated diphenyl ethers. *Chemosphere* **2014**, *111*, 7–12. [CrossRef] [PubMed]
30. Kovacevic, G.; Sabljic, A. Theoretical study on the mechanism and kinetics of addition of hydroxyl radicals to fluorobenzene. *J. Comput. Chem.* **2013**, *34*, 646–655. [CrossRef] [PubMed]
31. Kovacevic, G.; Sabljic, A. Mechanisms and reaction-path dynamics of hydroxyl radical reactions with aromatic hydrocarbons: The case of chlorobenzene. *Chemosphere* **2013**, *92*, 851–856. [CrossRef] [PubMed]
32. Kohn, W.; Becke, A.D.; Parr, R.G. Density functional theory of electronic structure. *J. Chem. Phys.* **1996**, *100*, 12974–12980. [CrossRef]

33. Becke, A.D. Density-functional thermochemistry. III. The role of exact exchange. *J. Chem. Phys.* **1993**, *98*, 5648–5652. [CrossRef]
34. Tomasi, J.; Mennucci, B.; Cammi, R. Quantum mechanical continuum solvation models. *Chem. Rev.* **2005**, *105*, 2999–3093. [CrossRef] [PubMed]
35. Burke, K.; Werschnik, J.; Gross, E.K.U. Time-dependent density functional theory: Past, present, and future. *J. Chem. Phys.* **2005**, *123*, 062206. [CrossRef] [PubMed]
36. Zhao, G.-J.; Han, K.-L. Excited state electronic structures and photochemistry of heterocyclic annulated perylene (HAP) materials tuned by heteroatoms: S, Se, N, O, C, Si, and B. *J. Phys. Chem. A* **2009**, *113*, 4788–4794. [CrossRef] [PubMed]
37. Zhao, G.-J.; Han, K.-L. Hydrogen bonding in the electronic excited state. *Acc. Chem. Res.* **2012**, *45*, 404–413. [CrossRef] [PubMed]
38. Albini, A.; Monti, S. Photophysics and photochemistry of fluoroquinolones. *Chem. Soc. Rev.* **2003**, *32*, 238–250. [CrossRef] [PubMed]
39. Fukui, K. The path of chemical reactions—The IRC approach. *Acc. Chem. Res.* **1981**, *14*, 363–368. [CrossRef]
40. Frisch, M.J.; Trucks, G.W.; Schlegel, H.B.; Scuseria, G.E.; Robb, M.A.; Cheeseman, J.R.; Scalmani, G.; Barone, V.; Mennucci, B.; Petersson, G.A.; et al. *Gaussian 09, Rev. B. 01*; Gaussian Inc.: Wallingford, CT, USA, 2009.
41. Qiang, Z.; Adams, C. Potentiometric determination of acid dissociation constants (p*K*a) for human and veterinary antibiotics. *Water Res.* **2004**, *38*, 2874–2890. [CrossRef] [PubMed]


**Sample Availability:** Samples of the compounds is not available from authors.